Journal of Biomolecular NMR, **22:** 47–56, 2002.
KLUWER/ESCOM

Structure refinement of flexible proteins using dipolar couplings: Application to the protein p8^{MTCP1}

Hélène Déméné*, Thierry Ducat, Philippe Barthe, Marc-André Delsuc & Christian Roumestand
Centre de Biochimie Structurale, UMR 5048 CNRS-UM1/UMR 554 INSERM-UM1, 15, avenue Charles Flahault, BP 14491, 34060 Montpellier Cedex 5, France

Received 24 September 2001; Accepted 19 October 2001

Abstract

The present study deals with the relevance of using mobility-averaged dipolar couplings for the structure refinement of flexible proteins. The 68-residue protein p8^{MTCP1} has been chosen as model for this study. Its solution state consists mainly of three α-helices. The two N-terminal helices are strapped in a well-determined α-hairpin, whereas, due to an intrinsic mobility, the position of the third helix is less well defined in the NMR structure. To further characterize the degrees of freedom of this helix, we have measured the dipolar coupling constants in the backbone of p8^{MTCP1} in a bicellar medium. We show here that including D_{HN}^{dip} dipolar couplings in the structure calculation protocol improves the structure of the α-hairpin but not the positioning of the third helix. This is due to the motional averaging of the dipolar couplings measured in the last helix. Performing two calculations with different force constants for the dipolar restraints highlights the inconstancy of these mobility-averaged dipolar couplings. Alternatively, prior to any structure calculations, comparing the values of the dipolar couplings measured in helix III to values back-calculated from an ideal helix demonstrates that they are atypical for a helix. This can be partly attributed to mobility effects since the inclusion of the ^{15}N relaxation derived order parameter allows for a better fit.

Introduction

Since their introduction in the field of high-resolution NMR (Tolman et al., 1995; Tjandra and Bax, 1997), dipolar couplings have been widely used for the determination and/or refinement of the structure of biomolecules. Including dipolar coupling constants in the structure calculations of medium-sized proteins improves the local geometry of peptide bonds (Bax et al., 1997; Arnesano et al., 2000). In case of larger proteins, when protein deuteration implies a minimal set of NOEs, the use of dipolar couplings leads to the drastic improvement of both accuracy and precision of the NMR derived structure (Clore et al., 1999; Huang et al., 2000; Mueller et al., 2000).

Another important feature of residual dipolar coupling restraints is the ability to establish the relative orientation of distant molecular fragments in modular proteins (Bewley and Clore, 2000; Skrynnikov et al., 2000). In these studies, it is generally assumed that dipolar couplings are measured between dipoles existing in a fixed, rigid geometry. Nevertheless, the relative orientation of secondary elements or larger domains in a protein is seldom fixed, due to the intrinsic backbone dynamics. It has been long recognized that dipolar couplings also reflect internal dynamics of protein (Tolman et al., 1995, 1997; Tsui et al., 2000). Correlation plots of dipolar couplings against R_2/R_1 values have been used to identify residues subject to conformational exchange in large anisotropic proteins (de Alba et al., 1999). Inter-domain motions have also been postulated to explain discrepancies between dipolar couplings measured in the individual domains of two modular proteins (Fischer et al., 1999; Skrynnikov et al., 2000).

It thus appears important to evaluate the contribution of this intrinsic mobility to the experimental values of dipolar couplings, as well as its consequential

*To whom correspondence should be addressed. E-mail: helene@cbs.univ-montp1.fr

effect on the 3D models deduced from these measurements. To this aim, we used the dipolar couplings measured on $p8^{MTCP1}$ to further investigate the structure and dynamics of this protein. $P8^{MTCP1}$ (Madani et al., 1995) is a small (68 residues) mitochondrial protein encoded by one of the two splicing forms of MTCP1, the first gene univocally identified in the group of uncommon leukemia with a mature phenotype (Stern et al., 1993). Previous reports on the structure of human $p8^{MTCP1}$ revealed an original scaffold consisting of three α-alpha helices, associated with a new cystein motif (Barthe et al., 1997, 1999) (Figure 1a). Two anti-parallel amphipatic helices spanning residues 8–20 (helix I) and residues 29–40 (helix II) are strapped in an α-hairpin motif by the two disulfide bridges 7–38 and 17–28. The third helix (helix III) spanning residues 48-63, is connected to this double-helix motif by a relatively well-defined loop (residues 41–46) and the third disulfide bridge 39–50. Probably due to an intrinsic flexibility, the relative orientation of helix III with respect to the α-hairpin is however poorly defined. Indeed, the presence of complex motions in helix III was clearly demonstrated by the analysis of ^{15}N relaxation data (Barthe et al., 1999; Canet et al., 2001). On the other hand, NMR measurements clearly established that the average structure of this segment is predominantly helicoïdal since typical (i, i+3) and $^{3}J_{HN}$ couplings < 5.5 Hz (Barthe et al., 1997, 1999) were observed. We present here the refinement of the structure of $p8^{MTCP1}$ using restraints deduced from the measurement of NH dipolar couplings. More importantly, we point out some deleterious effects due to the introduction of mobility-averaged dipolar couplings in the structure calculation. For all these last points, we think that our conclusions go beyond the frame of the structure refinement of $p8^{MTCP1}$ and should be relevant for any multi-domain proteins.

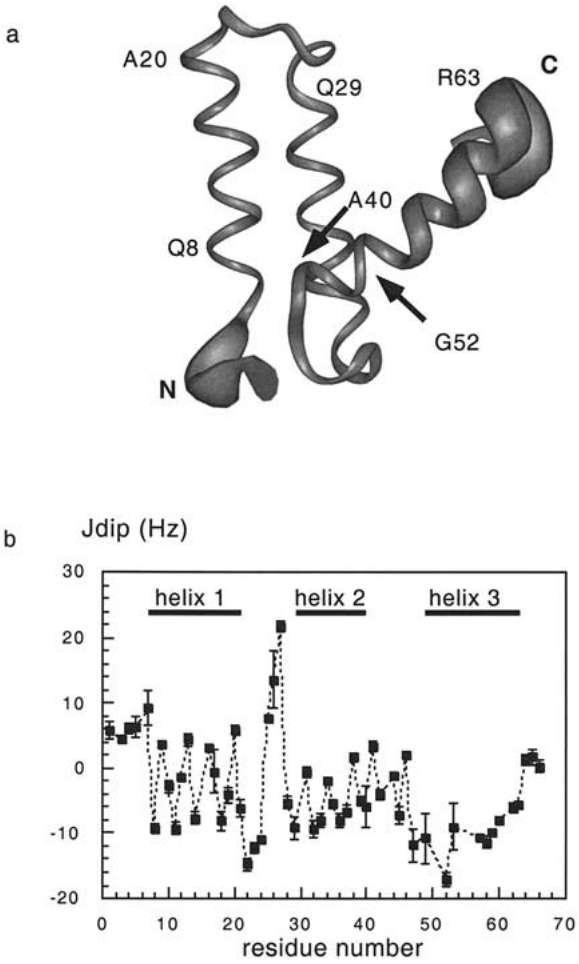

Figure 1. (a) ribbon representation of the backbone of the solution structure of $p8^{MTCP1}$. The value of the global order parameter S^2 is encoded in the width of the ribbon line. The N- and C-terminal ends of the protein are indicated in bold letters. (b) Experimental dipolar coupling constants as a function of residue number for $p8^{MTCP1}$. The position of the three helices is indicated as horizontal bold lines.

Materials and methods

Dipolar coupling measurements

The protein expression and purification has been described elsewhere (Barthe et al., 1999). The final concentration of ^{15}N labeled $p8^{MTCP1}$ in the NMR tube was 0.4 mM (pH 6.4). Experiments were run at 30 °C on an AMX 600 MHz Bruker spectrometer equipped with a z-gradient ^{1}H-^{13}C-^{15}N triple resonance probe. The D_{HN} couplings were measured on a bicelle-free tube and on a tube containing 7% (w/w) DLPC/CHAPSO (5:1) (Wang et al., 1998) as frequency differences in the t_1 dimension between the N+ and N- correlation peaks for each residue in the spectra recorded using the TROSY and anti-TROSY HSQC type experiments (Weigelt et al., 1998; Cordier et al., 1999). NMR experiments (256 complex t_1 × 1024 complex t_2 points) were processed using the Gifa software (Pons et al., 1996) to a final resolution of 1 Hz/pt. To increase the precision of the measure, the peak shape was then fitted using the Peak_fit routine in Gifa. The D_{HN}^{dip} dipolar couplings were obtained as differences between D_{HN}^{dip} splittings measured on the bicelle-free and bicelle containing solutions.

Structure calculations

Structures were calculated using the CNS software version 1.0 (Brünger et al., 1998) using the implemented protocol of simulated annealing. A high-temperature (50 000 K) simulated annealing protocol in torsion space starting from randomized coordinate positions was used for the first stages of structure calculations in which the NOE and dihedral angle restraints were included with constant forces of 150 kCal $Å^{-2}$ and 100 kCal rad^{-2} respectively. This was followed by a torsion slow-cool annealing stage cooling down the system to 0 K in step of 250 K. At each temperature step, 75 fs of molecular dynamics were recorded with a time-step of 15 fs. In addition, a Cartesian slow-cool annealing stage cooling down the system from 2000 K to 0 K in step of 25 K was performed. At each temperature step, 185 fs of molecular dynamics were recorded with a time-step of 5 fs. Structures were then subjected to 10 cycles of Powell minimization with the force constants set to 75 kCal $Å^{-2}$ and 400 kCal rad^{-2} for distance and dihedral restraints, respectively. For the calculations with dipolar coupling constraints, the dipolar coupling force constant was progressively raised to its final value K_{dip} during these two slow-cool annealing stages. The inclusion of dipolar restraints in structure calculations requires values of the parameters Aa and R, the axial and rhombic components of the alignment tensor. Rough estimates of these values were obtained from the fit of Equation 1 (*vide infra*) using the available NMR structures of $p8^{MTCP1}$. Preliminary calculations were then run to optimize the values of these parameters (Clore et al., 1998; Schwalbe et al., 2001). The values giving the lowest energies were selected for the final calculations (Aa = −12, R = 0.45).

In addition to the dipolar restraints free calculation, 3 calculations were performed using different sets of dipolar couplings. The first set includes 28 dipolar restraints, corresponding to NH groups located in helix I, helix II, and the N-terminal part of helix III (residues 49–52). This set corresponds to the residues that have been identified as rigid on the basis of NMR relaxation measurements (Barthe et al., 1999; Canet et al., 2001), and will be referred as 'minimal set' in the following. The second set contains 40 dipolar restraints corresponding to helix I, helix II, and helix III, and will be referred as 'rigid set' in the following. Finally, additional calculations were performed with a third set of dipolar splittings, identical to the 'rigid set' but with dipolar values inversely weighted by the NMR-derived order parameter S. This set will be referred as 'mobile set' in the following. The energy function for the dipolar restraints was a harmonic potential. For each dipolar set, we have used two different final force constants K_{dip} of 0.5 kcal mol^{-1} Hz^{-2} and 1.5 kcal mol^{-1} Hz^{-2}, since the results appeared to be dependent on this constant force. Both values belong to the interval defined in the literature (Clore and Garett, 1999) as producing acceptable structures. Typically, a set of 50 structures was generated for each calculation, and the 20 best ones in term of violation of experimental restraints were selected. In addition, the average structure over these 20 structures was calculated and minimized. Inspection and manipulation of the structures were made on a Silicon Graphic station with Insight (MSI, San Diego).

Model calculations

Independently from the structure calculations, dipolar couplings were fitted to alignment tensors by minimizing the function:

$$\chi^2 = \frac{1}{N-n}\sum_j \frac{\left\{\left(D_{HN}^{dip}\right)_{calc} - \left(D_{HN}^{dip}\right)_{meas}\right\}^2}{\left(\sigma_j^{dip}\right)^2},$$

where

$$\left(D_{HN}^{dip}\right)_{calc} = D\,A_a S\left(\left(3\cos^2\theta - 1\right) + 3/2R\sin^2\theta\,\cos(2\phi)\right), \quad (1)$$

N is the number of experimental constraints, n is the number of parameters to be optimized (here 5), σ_j is the measurement error,

$$\left(\sigma_j^{dip}\right)^2 = \left(\sigma_{N+}^2 + \sigma_{N-}^2\right)_{bicelles} + \left(\sigma_{N+}^2 + \sigma_{N-}^2\right)_{free},$$

$D = -(1/2\pi)(\mu_0/4\pi)(h/2\pi)\gamma_N\gamma_H r_{HN}^3$ is the dipolar interaction constant, S is the order parameter that reflects isotropic averaging (Tolman et al., 1997; Tsui et al., 2000), A_a is the axial component of the molecular alignment tensor, R is its rhombicity parameter and θ and ϕ are polar angles that specify the orientation of the HN vector with respect to the molecular alignment frame (Tjandra and Bax, 1997). The orientation of the alignment frame is defined relative to a fixed molecular frame, such as the NMR coordinate frame, and is expressed by the Euler angles (α, β, γ). Minimization

of the error function was performed using a simulated annealing algorithm as previously described (Déméné et al., 2000). R.m.s. deviations between simulated and experimental dipolar restraints were calculated with this program for the structures issued from CNS calculations, with the Aa and D parameters fixed to the previously determined values.

Results

Dipolar couplings measurement

Dipolar couplings were measured as described in the Material and Methods section. The experimental profile of the residual dipolar coupling constants versus the protein sequence is depicted on Figure 1b. The periodic profile of D_{HN}^{dip} couplings from residues 8 to 20 and 29 to 40 corresponds perfectly to what is expected for the two N-terminal helices of $p8^{MTCP1}$, the high similarity between the patterns obtained for the two helices being a result of their almost parallel disposition in the NMR derived structure (Barthe et al., 1999). By contrast, the dipolar couplings measured for residues 49–63 exhibit an atypical pattern for a helical structure, with negative values slowly increasing to zero from the N- to the C-terminal end of the helix.

Structure calculations without dipolar restraints for the mobile part of helix III: Effect of inclusion of dipolar restraints into structure calculations

The structure of $p8^{MTCP1}$ was calculated without and with dipolar restraints for helix I and II and the N-terminal part of helix III ('minimal set' – see Materials and methods). The structural statistics for both ensembles of structures are listed in Table 1. As previously reported (Clore et al., 1999; Huang et al., 2000; Schwalbe et al., 2001), inclusion of dipolar restraints increases the precision of the calculated structures: the mean backbone r.m.s.d. decreases from 0.48 to 0.42 and 0.36 when using a dipolar constant force of 0.5 and 1.5 kcal mol^{-1} Hz^{-2}, respectively. The PROCHECK analysis (Laskowski et al., 1993) shows that the percentage of residues lying in the most favored regions of the Ramachadran plot is slightly increased. This effect is more pronounced when using the lowest dipolar constant force value. On the other hand, inclusion of dipolar restraints causes a small increase in deviations from ideal covalent geometry. This effect has been already reported (Schwalbe et al., 2001) and is positively correlated with the value of K_{dip}. Finally, different behaviors are observed for the others experimental restraints (NOE-derived distances and ^{3}J-derived ϕ values): the energy term corresponding to distance restraints violations remains identical if not better, whereas the one corresponding to dihedral angles deviations is increased (but in an acceptable manner). All these conclusions are in agreement with calculations reported so far (Tjandra et al., 1997; Clore et al., 1999; Clore and Garett, 1999; Schwalbe et al., 2001).

From a strict structural point of view, inclusion of dipolar restraints in the calculations leads to a slight reorientation of helix II with respect to helix I. The mean angle between the axes of the two helices is 6.5 ± 4.04, 9.8 ± 2.5 and 14.5 ± 2.5 in the dipolar-free, in the low K_{dip} and in the high K_{dip}-based calculations, respectively. By calculating the Euler transformation which transposes helix I into helix II, we find in addition a small in-plane rotation of helix II around its principal axis. The relevant angle is -145 ± 2.25, -149 ± 2.1 and -152 ± 3.1, for the same three calculations, respectively. The average minimized structures issued from calculations with and without dipolar restraints ('minimal set', high K_{dip}) are superimposed on Figure 2.

Structure calculations including dipolar restraints for helix III: Effect of the motional averaging of dipolar couplings

The experimental profile of the dipolar couplings in helix III shows a pattern where the (negative) dipolar coupling constants increase slowly to zero without a net apparent periodicity. ^{15}N relaxation measurements have previously shown that HN bonds within helix III experience a complex motion (Barthe et al., 1999; Canet et al., 2001), with generalized order parameters S decreasing to zero from residue 54 to the C-terminal end. The relaxation-derived S^2 values are given as supplementary material.

Structure calculations were thus repeated, including the dipolar restraints for the mobile part of helix III. Two sets of calculations were performed, with S assumed to be equal to 1 ('rigid set') in Equation 1 or with the dipolar restraints inversely weighted by the S order parameter derived from previous ^{15}N NMR relaxation measurements ('mobile set'), this last calculations being likely to correspond more closely to the real situation. Again, the two different previously defined values of K_{dip} were used for the calculations.

Table 1. Structural statistics calculated for the 20 low-energy structures obtained without and with the 'minimal set' of dipolar couplings[a]

	Without dipolar coupling	With dipolar couplings[b] (high K_{dip})	With dipolar couplings[c] (low K_{dip})
RMS deviations from ideal covalent geometry			
Bonds (Å)	0.0056 ± 0.0004	0.0063 ± 0.0004	0.0058 ± 0.0003
Angles (deg)	0.652 ± 0.025	0.695 ± 0.037	0.658 ± 0.025
Improper (deg)	0.528 ± 0.029	0.563 ± 0.040	0.508 ± 0.039
RMS deviations from experimental restraints[d]			
Dihedral (deg)	0.126 ± 0.119	0.189 ± 0.156	0.156 ± 0.20
NOE (Å)	0.048 ± 0.003	0.045 ± 0.002	0.042 ± 0.003
Dipolar (Hz)	13.88 ± 4.60	0.07 ± 0.06	0.65 ± 0.20
Structural quality and coordinates precision			
Backbone RMSD to mean (Å) residues (8–63)	0.75 ± 0.27	0.80 ± 0.22	0.85 ± 0.21
Backbone RMSD to mean (Å) residues (8–20, 29–40 = helix I + helix II)	0.48 ± 0.12	0.36 ± 0.09	0.42 ± 0.10
Backbone RMSD to mean (Å) residues (49–63 = helix III)	0.57 ± 0.21	0.64 ± 0.19	0.59 ± 0.18
Percentage of residues in the most favoured regions of the Ramachadran plot[e]	83.5%	83.7%	85.0%

[a]The 'minimal' set corresponds to the dipolar couplings measured for residues 8–20 (helix I), 29–40 (helix II) and 49–52 (N-terminal part of helix III).
[b]Calculations were performed with a final value of 1.5 kcal mol^{-1} Hz^{-2} for the dipolar coupling force constant.
[c]Calculations were performed with a final value of 0.5 kcal mol^{-1} Hz^{-2} for the dipolar coupling force constant.
[d]No structure presents NOE violations >0.5 Å or dihedral violations >5°. Calculations with a high K_{dip} and low K_{dip} yield 0 and 0–2 dipolar violations >2 Hz, respectively.
[e]Calculated with the program PROCHECK (Laskowski et al., 1993).

Back-calculated dipolar couplings obtained from the different calculations are plotted in Figure 3 versus the protein sequence and Table 2 lists the structural statistics obtained for all structure ensembles.

Surprisingly, although one would expect to obtain more realistic structures, identical conclusions can be drawn from structures obtained with either the 'mobile set' or the 'rigid' set of dipolar couplings (Table 2). In particular, in spite of significant differences between the weighted and non-weighted values of D_{HN}^{dip} in helix III, all calculations performed using the high K_{dip} value converge successfully to structures possessing acceptable geometry and fulfilling all experimental data (NOEs, J couplings and dipolar couplings). As compared to structure calculations performed with the 'minimal set' of dipolar couplings, adding the dipolar restraints (rigid or mobile set) measured in the mobile part of helix III in the structure refinement affects the statistics in different ways. In terms of deviations from ideal geometry, the percentage of residues lying in the most favored regions of the Ramachadran plot remains identical. Similarly, the number and the magnitude of NOEs violations are unchanged. On the other hand, one observes an increase of the number of the dihedral violations, especially when the high K_{dip} value is used. Nevertheless, even in this case, deviations remain in acceptable limits (no violations > 5°). Considering dipolar couplings, significant violations are observed in helix III between experimental and back-calculated values, even though the use of the high K_{dip} value yields acceptable deviations. Finally, in terms of precision of the structures, backbone r.m.s.d. for the segments (8–63) (helix I + helix II + helix III) and (49–63) (helix III) remain similar (high K_{dip} value), indicating that there is no improvement neither in the positioning of helix III with respect to the hairpin motif nor in the local definition of the helix. Nevertheless, calculations with the low K_{dip} value yield structures presenting a somehow better definition, but as mentioned above, at the expense of severe violations of the experimental dipolar couplings.

In order to better appreciate a potential improvement of the local structure in the different helices, a comparison has been made between each helical seg-

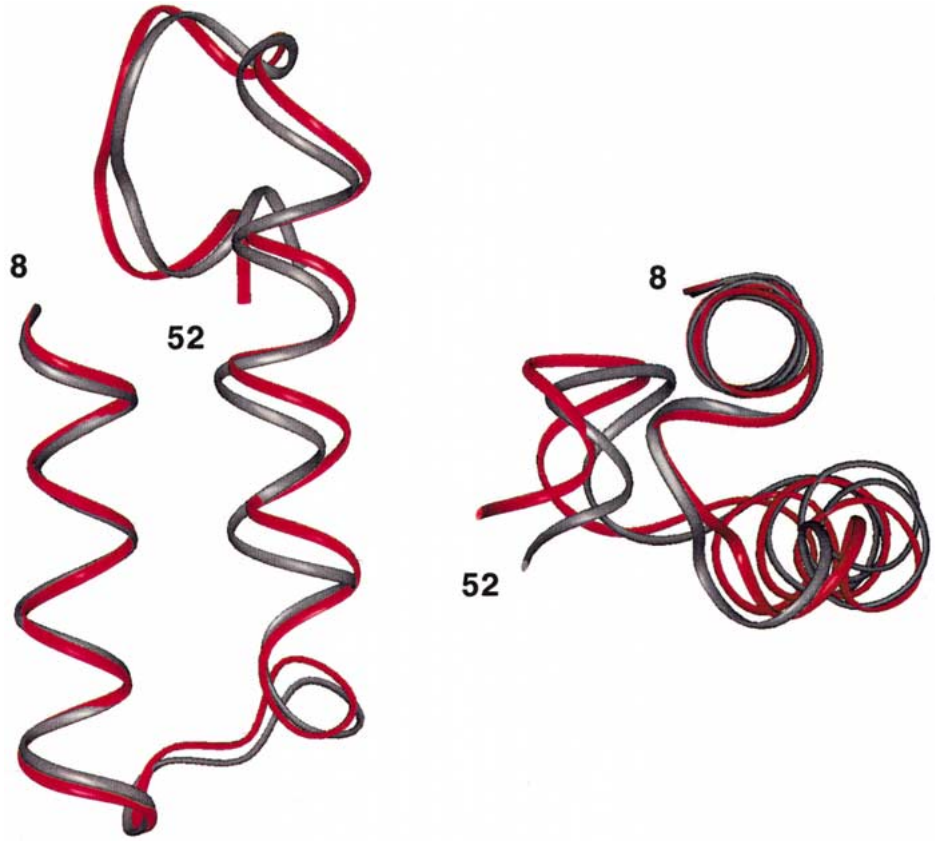

Figure 2. Superimposition of the average structures (ribbon representation) of the α-hairpin in the $p8^{MTCP1}$ solution structures issued from CNS calculations without dipolar restraints (black) and with dipolar restraints (red) ('minimal set' = helix I + helix II + residues 49–53, high K_{dip}). The two views are 90°-rotated around an axis perpendicular to the α-hairpin main axis. The superimposition has been enforced on helix I residues (8–20) in order to highlight the reorientation of helix II (residues 29–40) upon inclusion of dipolar couplings.

ment in the different models (no dipolar, 'minimal', 'rigid' and 'mobile' set) and ideal helices (Creighton, 1993). Table 3 summarizes the pairwise backbone atoms r.m.s.d. values measured between ideal helices and the corresponding helices in the structure of $p8^{MTCP1}$ obtained from the different calculations. As a first result, including dipolar couplings in the CNS calculations improves the geometry of helix I and II toward what is expected for an ideal helix. By contrast, inclusion of dipolar couplings for helix III leads to a pronounced distortion, especially when dipolar coupling are not weighted with the NMR-derived order parameter. From a structural point of view, this is the sole evidence of a 'positive' discrimination between the 'rigid' set and the 'mobile' set in the CNS calculations.

To summarize, it appears that including mobility-averaged dipolar couplings in structure calculations gives rise to local structures presenting acceptable statistics and geometry but does not improve – if not damage – the quality of the global structure. Trying to account for flexibility by including the order parameter in the calculations with the dipolar couplings does not yield any substantial improvements. Although the rigid set and the mobile sets yield acceptable structures, the cost is a deviation of the structure of helix III from ideality, particularly for the rigid set.

Fitting dipolar restraints against ideal secondary elements

Figure 4 displays the experimental values of the dipolar couplings as well as the simulated dipolar couplings deduced from the coordinates of the NH bonds of ideal helices individually fitted on each helix of $p8^{MTCP1}$. For this particular calculation, all the components of the alignment tensor were optimized (orientation and magnitude) (see Materials and methods).

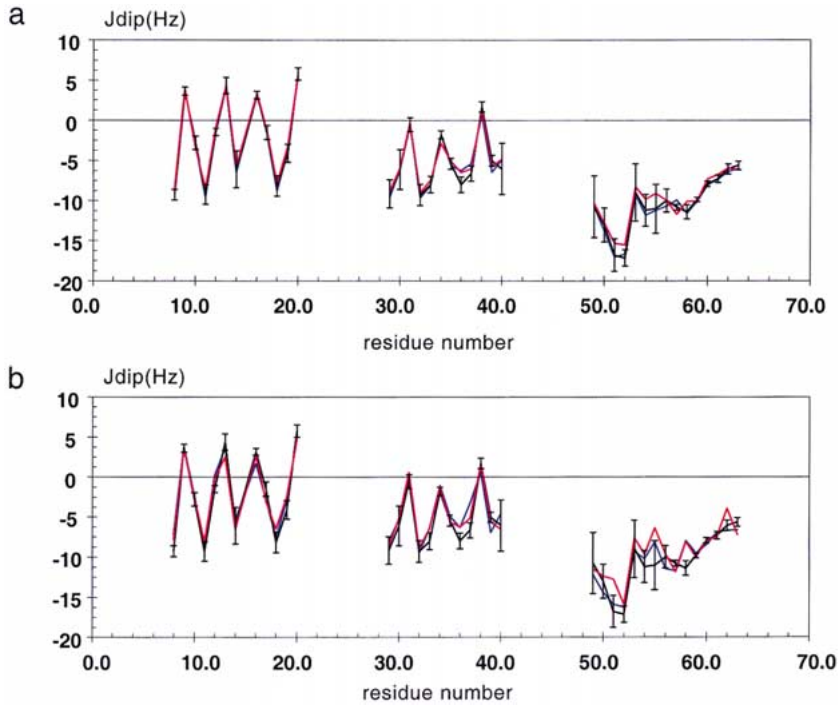

Figure 3. Experimental (black lines) and back-calculated dipolar coupling constants as a function of the residue number in the sequence considering the HN bonds as rigid in helix III (red lines), or taking into account the NMR derived experimental order parameters in Equation 1 (blue lines). Calculations have been performed using the coordinates of the CNS structures with a high K_{dip} value, 1.5 kCal mol^{-1} H_3^{-2} (a) and a low K_{dip} value, 0.5 kCal mol^{-1} H_3^{-2} (b).

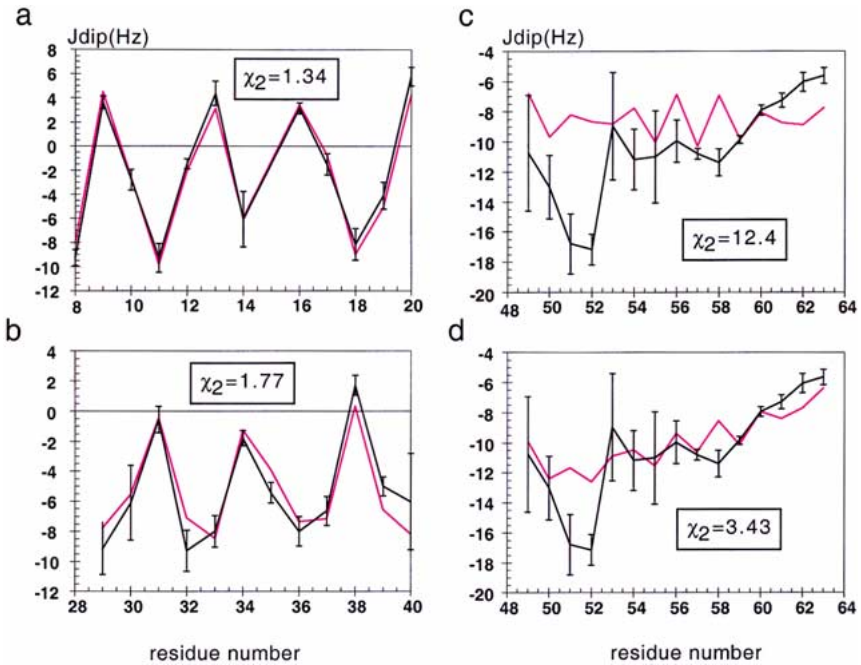

Figure 4. The experimental dipolar couplings of helix I (a), helix II (b) and helix III (c) are fitted to the alignment tensor calculated from the coordinates of an ideal helix (see Materials and methods) considering the NH bonds as rigid (S=1). In (d), the fit is performed considering the NH bonds of helix III are mobile ($S=S^{NMR}$ in Equation 1). For these particular calculations, optimization of the tensor alignment concern all components (orientation and magnitude).

Table 2. Structural statistics calculated for the 20 low-energy structures obtained with the 'rigid' and the 'mobile' sets of dipolar couplings[a]

	Rigid set + high K^b_{dip}	Rigid set + low K^c_{dip}	Mobile set + high K^b_{dip}	Mobile set + low K^c_{dip}
RMS deviations from ideal covalent geometry				
Bonds (Å)	0.0065 ± 0.0003	0.0061 ± 0.0003	0.0063 ± 0.0004	0.00059 ± 0.000
Angles (deg)	0.730 ± 0.026	0.680 ± 0.030	0.715 ± 0.030	0.663 ± 0.031
Impropers (deg)	0.617 ± 0.022	0.524 ± 0.033	0.594 ± 0.034	0.521 ± 0.034
RMS deviations from experimental restraints[d]				
Dihedral (deg)	0.282 ± 0.025	0.141 ± 0.115	0.245 ± 0.143	0.125 ± 0.016
NOE (Å)	0.047 ± 0.000	0.044 ± 0.002	0.046 ± 0.004	0.042 ± 0.003
Dipolar (Hz)	0.23 ± 0.14	0.95 ± 0.20	0.31 ± 0.28	0.63 ± 0.15
Structural quality and coordinates precision				
Backbone RMSD to mean (Å) residues (8–63)	0.77 ± 0.25	0.60 ± 0.30	0.83 ± 0.22	0.64 ± 0.13
Backbone RMSD to mean (Å) residues (8–20, 29–40 = helix I + helix II)	0.40 ± 0.11	0.37 ± 0.14	0.38 ± 0.10	0.37 ± 0.11
Backbone RMSD to mean (Å) residues (49–63 = helix III)	0.69 ± 0.26	0.41 ± 0.13	0.68 ± 0.11	0.62 ± 0.18
Percentage of residues in the most favored regions of the Ramachadran plot[e]	83.2%	83.6%	84.4%	82.3%

[a]The mobile and rigid sets correspond to the dipolar couplings measured for residues 8–20 (helix I), 29–40 (helix II) and 49–63 (helix III).
[b]Calculations were performed with a final value of 1.5 kcal mol^{-1} Hz^{-2} for the dipolar coupling force constant.
[c]Calculations were performed with a final value of 0.5 kcal mol^{-1} Hz^{-2} for the dipolar coupling force constant.
[d]No structure presents NOE violations > 0.5Å or dihedral violations >5°. Calculations with a high K_{dip} and low K_{dip} yield 0–2 and 4–8 dipolar violations >2 Hz, respectively.
[e]Calculated with the program PROCHECK (Laskowski et al., 1993).

Table 3. Pairwise backbone r.m.s. deviations measured between an ideal helix and each helix of the minimized average structures resulting from the different calculations

	Helix I	Helix II	Helix III
No dipolar couplings	0.516	0.742	0.896
With dipolar couplings 'minimal set', high K^a_{dip}	0.375	0.515	0.947
With dipolar couplings 'minimal set', low K^b_{dip}	0.388	0.377	0.771
With dipolar couplings 'rigid set', high K^a_{dip}	0.404	0.504	1.680
With dipolar couplings 'rigid set', low K^b_{dip}	0.389	0.695	1.561
With dipolar couplings 'mobile set', high K^a_{dip}	0.388	0.501	1.153
With dipolar couplings 'mobile set', low K^b_{dip}	0.368	0.645	1.234

[a]Calculations were performed with a final value of 1.5 kcal $mol^{-1}Hz^{-2}$ for the dipolar coupling force constant.
[b]Calculations were performed with a final value of 0.5 kcal $mol^{-1}Hz^{-2}$ for the dipolar coupling force constant.

For helix I and II, the individual fits give good normalized χ^2 values of 1.34 and 1.77 respectively (Figures 4a and 4b). Beside any structure calculations, the excellent agreement between experimental and simulated dipolar couplings indicates that helices I and II are very close to ideal helices. By contrast, a bad χ^2 value (12.40) is obtained for helix III. Such a bad value may come either from the fact that the mean structure of helix III is not ideal, as suggested by our structures calculations including dipolar couplings, or/and from the effect of the intrinsic flexibility of this segment, as suggested by our previous studies (Barthe et al., 1999; Canet et al., 2001). Weighting the dipolar restraints by the NMR relaxation derived order parameter leads to a drastic decrease of the χ^2 value (3.43). This strongly suggests that an important part of the discrepancies observed between the experimental dipolar coupling values in helix III and the back-calculated values based on an ideal helix comes from the contribution of the flexibility sensed by the ^{15}N heteronuclear relaxation parameters.

Discussion and conclusion

Previous studies have shown that the orientation of helix III with respect to the α-hairpin in the refined solution structure of $p8^{MTCP1}$ cannot be defined precisely only with NOEs or scalar coupling derived distance and angular restraints (Barthe et al., 1999). Deep insights in the backbone dynamics of the protein based on ^{15}N relaxation studies have then suggested that this ill-definition was due to an intrinsic flexibility of helix III (Barthe et al., 1999; Canet et al., 2001). The present study reports the refinement of the structure of $p8^{MTCP1}$ using dipolar couplings derived restraints, the final aim being to draw more general conclusions about the relevance of these couplings when they are measured on flexible segments.

As compared to the previous ensemble of NMR structures, there is a need for a slight mutual reorientation of helices I and II to account for dipolar couplings. The required reorientation is small (+4 to +8 deg), yielding a geometry close to what observed in canonical coiled-coils (20°, Schultz and Schirmer, 1979). In addition, a better agreement is obtained between experimental and back-calculated dipolar couplings for helix II after a slight in-plane reorientation of this helix. Hence, this study is another clear demonstration of the usefulness of dipolar coupling restraints to monitor the orientation of rigid elements inside small proteins and peptides where NOEs are sparse by nature.

On the other hand, as a result of motional averaging, the positioning of helix III with respect to the α-hairpin cannot be specified further from the inclusion in the calculations of the experimental dipolar couplings measured in this mobile segment. Moreover, calculations with these dipolar couplings yield structures where helix III is distorted, in contradiction with preliminary NMR studies that suggest a more or less canonical geometry for helix III (Barthe et al., 1997, 1999). Interestingly, a geometry closer to what expected for an ideal helix is obtained when weighting with the order parameter issued from relaxation studies. Nevertheless, no significant differences in any energy terms could be found in the structural statistics of the calculated structural ensembles allowing an irrefutable discrimination between weighted or non-weighted data. Recent theorical studies (Tsui et al., 2000; Tolman et al., 2001; Meiler et al., 2001) suggest that such a result is expected when the HN bonds exhibit anisotropic motions or motions slower than the tumbling rate of the molecule.

On the other hand, the significant improvement of the fits when considering the NMR order parameter S for the back-calculation of the dipolar couplings from coordinates of ideal helices indicates that an important part of mobility for helix III is sensed by the measured heteronuclear relaxation parameters, with the implication that the relevant motion is faster than the overall correlation time. This is consistent with previous results obtained from a multiple-fields relaxation analysis of p8 that have demonstrated that slow motions, related to conformational exchange, were essentially limited to the side-chain reorientation of aromatic residues (Tyr23, Phe50) located in the loops joining the different helices (Canet et al., 2001). Thus, weighting the measured dipolar data for helix III by the ^{15}N relaxation-derived order parameter should give a correct estimation of the motional averaging experienced by the C-terminal part of helix III of $p8^{MTCP1}$. The residual discrepancy between simulated and experimental dipolar couplings may then come from the anisotropy of the motion sensed by the dipolar couplings (Tsui et al., 2000) or from slight deviations of the geometry of helix III from ideality. The exact explanation will require more measurements of dipolar couplings, either between other atoms or in other media, as suggested in recent studies (Tolman et al., 2001; Meiler et al., 2001). Note that these studies require the measurement of an extensive set of dipolar couplings: Six values by peptidic plane for Tolman et al., nine different alignment media for Meiler et al.

From our different attempts to introduce mobility-averaged dipolar couplings in the structure calculation of $p8^{MTCP1}$, we draw the following conclusions:

– It is easy in the process of structure calculations to accommodate for 'wrong' dipolar couplings, without high violations of other experimental parameters or ideal geometry. Clore and Garett (Clore and Garett, 1999) have established an interval of K_{dip} values (0.2–2.25 kcal mol^{-1} Hz^{-2}) compatible with CNS structure calculations. On the basis of our calculations, we would recommend to exclude the higher values of this interval. The discrepancies between the two studies stem obviously from the fact that Clore and Garett have used dipolar couplings where the flexibility effects could be neglected, so that using higher values of K_{dip} still leads to valid results.

– On the other hand, repeating structures calculations with two different K_{dip} values gives insight into the consistency of the experimental dipolar couplings. In our study, the sole hint that we use inadequate dipo-

lar couplings is that using a higher K_{dip} value slightly *decreases* the precision of the calculated structures, in complete contradiction with what is usually observed. This result was confirmed when using a higher value for K_{dip} (2.25 kcal mol^{-1} Hz^{-2}; data not shown).

We think that these conclusions might be relevant for others flexible proteins.

Acknowledgements

The authors want to thank Patrice Dosset for his indispensable programming skill and Marie-Paule Strub for her technical assistance in the protein expression. This work was partly supported by grants from the Association pour la Recherche sur le Cancer.

References

Arnesano, F., Banci, L., Bertini, I., van der Wetering, K., Czisch, M. and Kaptein, R. (2000) *J. Biomol. NMR*, **17**, 295–304.

Barthe, P., Chiche, L., Declerck, N., Delsuc, M.A.D., Lefèvre, J.F., Malliavin, T., Mispelter, J., Stern, M.A., Lhoste, J.M. and Roumestand, C. (1999) *J. Biomol. NMR*, **15**, 271–288.

Barthe, P., Yang, Y., Chiche, L., Hoh, F., Strub, M.P., Guignard, L., Soulier, J., Stern, M.H., van Tilbeurgh, H., Lhoste, J.M. and Roumestand, C. (1997) *J. Mol. Biol.*, **274**, 801–815.

Bax, A. and Tjandra, N. (1997) *J. Biomol. NMR*, **3**, 289–292.

Bewley, C. and Clore, G.M. (2000) *J. Am. Chem. Soc.*, **122**, 6009–6016.

Brünger, A.T., Adams, P.D., Clore, G.M., DeLano, W.L., Gros, P., Grosse-Kunstleve, R.W., Jiang, J.S., Kuszewski, J., Nilges, M., Pannu, N.S., Read, R.J., Rice, L.M., Simonson, T. and Warren, G.L. (1998) *Acta Cryst.*, **54**, 905–921.

Canet, D., Barthe, P., Mutzenhardt, P. and Roumestand, C. (2001) *J. Am. Chem. Soc.*, **123**, 4567–4576.

Clore, G.M. and Garett, D.S. (1999) *J. Am. Chem. Soc.*, **121**, 9008–9012.

Clore, G.M., Gronenborn, A.M. and Tjandra, N. (1998) *J. Magn. Reson.*, **131**, 159–162.

Clore, G.M., Starich, M.R., Bewley, C.A., Cai, M. and Kuszewski, J. (1999) *J. Am. Chem. Soc.*, **121**, 6513–6514.

Cordier, F., Dingley, A.J. and Grzesiek, S. (1999) *J. Biomol. NMR*, **13**, 175–180.

Creighton, T.E. (1993) *Proteins: Structures and Molecular Properties*, W.H. Freeman and Co., San Francisco, p. 183.

de Alba, E., Baber, J.L. and Tjandra, N. (1999) *J. Am. Chem. Soc.*, **121**, 4282–4283.

Déméné, H., Tsan, P., Gans, P. and Marion, D. (2000) *J. Phys. Chem.*, **B104**, 2559–2569.

Fischer, M. W. F., Losonczi, J.A., Weaver J.L. and Prestegard J.H. (1999) *Biochemistry*, **38**, 9013–9022.

Huang, X., Moy, F. and Powers, R. (2000) *Biochemistry*, **39**, 13365–13375.

Leskowski, R.A., MacArthur, M.W., Moss, D.S. and Thornton, J.M. (1993) *J. Appl. Crystallogr.*, **26**, 283–291.

Madani, A., Soulier, J., Schmid, M., Plichtova, R., Lermé, F., Gateau-Roesch, O., Garnier, J.P., Pla, M., Sigaux, F. and Stern, M.-H. (1995) *Oncogene*, **10**, 2259–2262.

Meiler, J., Prompers, J.J., Peti, W., Griesinger, C. and Brüschweiler, R. (2001) *J. Am. Chem. Soc.*, **123**, 6098–6107.

Mueller, G. A., Choy, W.Y., Yang, D., Forman-Kay, J., Venters, R.A. and Kay, L.E. (2000) *J. Mol. Biol.*, **300**, 197–212.

Pons, J. L., Malliavin, T. and Delsuc, M.A.D. (1996) *J. Biomol. NMR*, **8**, 445–452.

Schwalbe, H., Grimshaw, S.B., Spencer, A., Buck, M., Boyd, J., Dobson, C.M., Redfield, C. and Smith, L.J. (2001) *Protein Sci.*, **10**, 677–688.

Schultz, G.E. and Schirmer, R.H. (1979) *Principles of Protein Structure*, Springer-Verlag, New York, pp. 79–81.

Skrynnikov, N. R., Goto, N.K., Yang, D., Choy, W.Y., Tolman, J.R., Mueller, G.A. and Kay, L.E. (2000) *J. Mol. Biol.*, **295**, 1265–1273.

Stern, M. H., Soulier, J., Rosenwajg, M., Nakahara, K., Canki-Klain, N., Aurias, S., Sigaux F. and Kirsch, I.R. (1993) *Oncongene*, **8**, 2475–2483.

Tjandra, N. and Bax, A. (1997) *Science*, **278**, 1111–1114.

Tolman, J.R., Al-Hashimi, H.M., Kay, L.E. and Prestegard, J.H. (2001) *J. Am. Chem. Soc.*, **123**, 1416–1424.

Tolman, J.R., Flanagan, J.M., Kennedy, M.A. and Prestegard, J.H. (1995) *Proc. Natl. Acad. Sci. USA*, **92**, 9279–9283.

Tolman, J. R., Flaganan, J.M., Kennedy, M.A. and Prestegard, J.H. (1997) *Nat. Struct. Biol.*, **5**, 292–297.

Tsui, V., Zhu, L., Huang, T.H., Wright, P.E. and Case, D.A. (2000) *J. Biomol. NMR*, **1**, 9–21.

Wang, H., Eberstqdt, M., Olejniczak, E.T., Meadow, R.P. and Fesik, S.W. (1998) *J. Biomol. NMR*, **12**, 443–446.

Weigelt, J. (1998) *J. Am. Chem. Soc.*, **120**, 10778–10779.